

# A small proton charge radius from an electron–proton scattering experiment

<https://doi.org/10.1038/s41586-019-1721-2>

Received: 17 June 2019

Accepted: 19 September 2019

Published online: 6 November 2019

W. Xiong<sup>1</sup>, A. Gasparian<sup>2\*</sup>, H. Gao<sup>1</sup>, D. Dutta<sup>3\*</sup>, M. Khandaker<sup>4</sup>, N. Liyanage<sup>5</sup>, E. Pasyuk<sup>6</sup>, C. Peng<sup>1</sup>, X. Bai<sup>5</sup>, L. Ye<sup>3</sup>, K. Gnanvo<sup>5</sup>, C. Gu<sup>1</sup>, M. Levillain<sup>2</sup>, X. Yan<sup>1</sup>, D. W. Higinbotham<sup>6</sup>, M. Meziane<sup>1</sup>, Z. Ye<sup>1,7</sup>, K. Adhikari<sup>3</sup>, B. Aljawrneh<sup>2</sup>, H. Bhatt<sup>3</sup>, D. Bhetuwal<sup>3</sup>, J. Brock<sup>6</sup>, V. Burkert<sup>6</sup>, C. Carlin<sup>6</sup>, A. Deur<sup>6</sup>, D. Di<sup>5</sup>, J. Dunne<sup>3</sup>, P. Ekanayaka<sup>3</sup>, L. El-Fassi<sup>3</sup>, B. Emmich<sup>3</sup>, L. Gan<sup>8</sup>, O. Glamazdin<sup>9</sup>, M. L. Kabir<sup>3</sup>, A. Karki<sup>3</sup>, C. Keith<sup>6</sup>, S. Kowalski<sup>10</sup>, V. Lagerquist<sup>11</sup>, I. Larin<sup>12,13</sup>, T. Liu<sup>1</sup>, A. Liyanage<sup>14</sup>, J. Maxwell<sup>6</sup>, D. Meekins<sup>6</sup>, S. J. Nazeer<sup>14</sup>, V. Nelyubin<sup>5</sup>, H. Nguyen<sup>5</sup>, R. Pedroni<sup>2</sup>, C. Perdrisat<sup>15</sup>, J. Pierce<sup>6</sup>, V. Punjabi<sup>16</sup>, M. Shabestari<sup>3</sup>, A. Shahinyan<sup>17</sup>, R. Silwal<sup>10</sup>, S. Stepanyan<sup>6</sup>, A. Subedi<sup>3</sup>, V. V. Tarasov<sup>12</sup>, N. Ton<sup>5</sup>, Y. Zhang<sup>1</sup> & Z. W. Zhao<sup>1</sup>

Elastic electron–proton scattering (e–p) and the spectroscopy of hydrogen atoms are the two methods traditionally used to determine the proton charge radius,  $r_p$ . In 2010, a new method using muonic hydrogen atoms<sup>1</sup> found a substantial discrepancy compared with previous results<sup>2</sup>, which became known as the ‘proton radius puzzle’. Despite experimental and theoretical efforts, the puzzle remains unresolved. In fact, there is a discrepancy between the two most recent spectroscopic measurements conducted on ordinary hydrogen<sup>3,4</sup>. Here we report on the proton charge radius experiment at Jefferson Laboratory (PRad), a high-precision e–p experiment that was established after the discrepancy was identified. We used a magnetic-spectrometer-free method along with a windowless hydrogen gas target, which overcame several limitations of previous e–p experiments and enabled measurements at very small forward-scattering angles. Our result,  $r_p = 0.831 \pm 0.007_{\text{stat}} \pm 0.012_{\text{sys}}$  femtometres, is smaller than the most recent high-precision e–p measurement<sup>5</sup> and 2.7 standard deviations smaller than the average of all e–p experimental results<sup>6</sup>. The smaller  $r_p$  we have now measured supports the value found by two previous muonic hydrogen experiments<sup>1,7</sup>. In addition, our finding agrees with the revised value (announced in 2019) for the Rydberg constant<sup>8</sup>—one of the most accurately evaluated fundamental constants in physics.

The proton is the dominant component of visible matter in the Universe. Consequently, determining the proton’s basic properties—such as its root-mean-square charge radius,  $r_p$ —is of interest in its own right. Accurate knowledge of  $r_p$  is also important for the precise determination of other fundamental constants, such as the Rydberg constant ( $R_\infty$ )<sup>2</sup>. The value of  $r_p$  is also required for precise calculations of the energy levels and transition energies of the hydrogen atom—for example, the Lamb shift. In muonic hydrogen ( $\mu\text{H}$  atoms), in which the electron in the H atom is replaced by a ‘heavier electron’ (a muon), the extended proton charge distribution changes the Lamb shift by as much as 2%<sup>1</sup>. The first-principles calculation of  $r_p$  from the accepted theory of the strong interaction (quantum chromodynamics, QCD), is notoriously challenging and currently cannot reach the accuracy demanded by experiments, but lattice QCD calculations are on the cusp of becoming precise enough to be tested experimentally<sup>9</sup>. Therefore, the precise measurement of  $r_p$  is not only critical for addressing the proton radius

puzzle but also important for determining certain fundamental constants of physics and testing lattice QCD.

Prior to 2010 the two methods used to measure  $r_p$  were ep elastic scattering measurements, in which the slope of the extracted proton (p) electric (E) form factor,  $G_E^p$ , as the four-momentum transfer squared ( $Q^2$ ) approaches zero, is proportional to  $r_p^2$ ; and Lamb shift (spectroscopy) measurements of ordinary H atoms, which, along with state-of-the-art calculations, can be used to determine  $r_p$ . Although the e–p results can be somewhat less precise than the spectroscopy results, until 2010 the values of  $r_p$  obtained from these two methods<sup>2,5</sup> mostly agreed with each other<sup>10</sup>. Since that year, two new results based on Lamb shift measurements in  $\mu\text{H}$  were reported<sup>1,7</sup>. The Lamb shift in  $\mu\text{H}$  is several million times more sensitive to  $r_p$  because the muon in a  $\mu\text{H}$  atom is about 200 times closer to the proton than is the electron in a H atom. To the surprise of both the nuclear and atomic physics communities, the two  $\mu\text{H}$  results<sup>1,7</sup>, displaying unprecedented precision with an estimated uncertainty of

<sup>1</sup>Duke University and Triangle Universities Nuclear Laboratory, Durham, NC, USA. <sup>2</sup>North Carolina A&T State University, Greensboro, NC, USA. <sup>3</sup>Mississippi State University, Mississippi State, MS, USA. <sup>4</sup>Idaho State University, Pocatello, ID, USA. <sup>5</sup>University of Virginia, Charlottesville, VA, USA. <sup>6</sup>Thomas Jefferson National Accelerator Facility, Newport News, VA, USA. <sup>7</sup>Argonne National Laboratory, Lemont, IL, USA. <sup>8</sup>University of North Carolina, Wilmington, NC, USA. <sup>9</sup>Kharkov Institute of Physics and Technology, Kharkov, Ukraine. <sup>10</sup>Massachusetts Institute of Technology, Cambridge, MA, USA. <sup>11</sup>Old Dominion University, Norfolk, VA, USA. <sup>12</sup>Alikhanov Institute for Theoretical and Experimental Physics NRC “Kurchatov Institute”, Moscow, Russia. <sup>13</sup>University of Massachusetts, Amherst, MA, USA. <sup>14</sup>Hampton University, Hampton, VA, USA. <sup>15</sup>College of William and Mary, Williamsburg, VA, USA. <sup>16</sup>Norfolk State University, Norfolk, VA, USA. <sup>17</sup>Yerevan Physics Institute, Yerevan, Armenia. \*e-mail: gasparan@jlab.org; d.dutta@msstate.edu

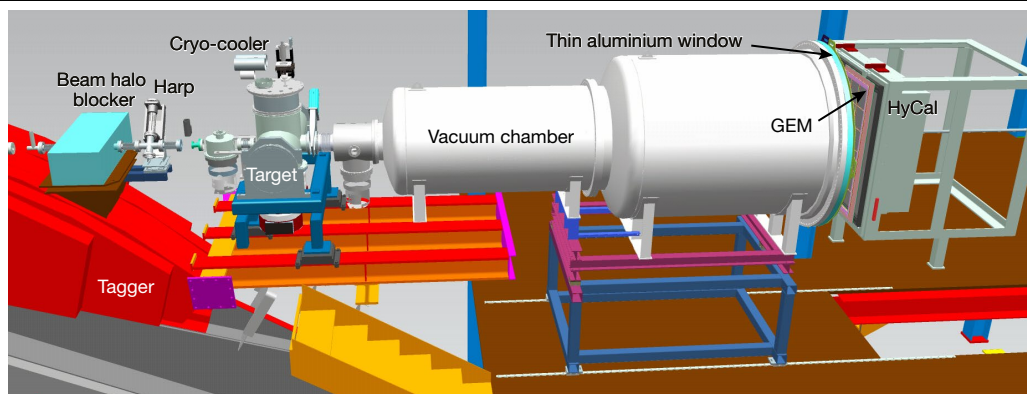


**Fig. 1 | The PRad experimental setup.** A schematic layout of the PRad experimental setup in Hall B at Jefferson Laboratory, with the electron beam incident from the left. The key beam-line elements are shown along with the

windowless hydrogen gas target, the two-segment vacuum chamber and the two detector systems (see the Methods for a brief overview and the Supplementary Information for a description of the target and individual detectors).

<0.1%, combined to be eight standard deviations smaller than the average value obtained from all previous experiments. This became known as the proton radius puzzle<sup>11</sup>, unleashing intensive experimental and theoretical efforts aimed at resolving the disagreement.

The discrepancy between the values of  $r_p$  as measured in H and  $\mu$ H atoms remains unresolved. Moreover, the two most recent H spectroscopy measurements disagree with each other<sup>3,4</sup>, which has added a new dimension to and renewed the urgency of this problem. A fundamental difference between the e-p and  $\mu$ -p interactions could be the origin of the discrepancy; however, there are abundant experimental constraints on any such 'new physics', although models that resolve the puzzle by invoking new force carriers have been proposed<sup>11,12</sup>. More mundane solutions continue to be explored: for example, it has been rigorously shown that the definition of  $r_p$  used in all three major experimental approaches was consistent<sup>13</sup>. The effect of two-photon exchange on  $\mu$ H spectroscopy<sup>14,15</sup>, and form-factor nonlinearities in e-p scattering<sup>16-18</sup> have also been examined. None of these studies has adequately explained the puzzle, reinforcing the need for additional high-precision measurements of  $r_p$  that use new experimental techniques and different systematics.

The PRad collaboration at Jefferson Laboratory has developed and performed an e-p experiment as an independent measurement of  $r_p$  to address the puzzle. The PRad experiment, in contrast with previous e-p experiments, was designed to use a magnetic-spectrometer-free, calorimeter-based method<sup>19</sup>. The design of the PRad experiment implemented three major improvements over previous e-p experiments. First, the large angular acceptance (0.7°–7.0°) of the hybrid calorimeter (HyCal) enabled large  $Q^2$  coverage, spanning two orders of magnitude ( $2.1 \times 10^{-4} \text{ GeV}^2/c^2$  to  $6 \times 10^{-2} \text{ GeV}^2/c^2$ , where  $c$  is the speed of light in a vacuum) in the low  $Q^2$  range. The fixed location of HyCal eliminated the many normalization parameters that plague magnetic-spectrometer-based experiments in which the spectrometer must be physically moved to many different angles to cover the desired range of  $Q^2$ . In addition, the PRad experiment reached extreme forward-scattering angles of down to 0.7°, achieving a  $Q^2$  value of  $2.1 \times 10^{-4} \text{ GeV}^2/c^2$ ; this is, to our knowledge, the lowest  $Q^2$  obtained from e-p experiments and is an order of magnitude lower than that previously achieved<sup>5</sup>. Reaching a lower range for  $Q^2$  is critical because  $r_p$  is determined from the slope of the electric form factor at  $Q^2 = 0$ . Second, the extracted e-p cross-sections were normalized to the well-known quantum electrodynamics process  $e^-e^- \rightarrow e^-e^-$  (Møller scattering from atomic electrons, e-e), which was measured simultaneously alongside e-p scattering, using the same detector acceptance. This led to a substantial reduction in the systematic uncertainties of measuring the e-p cross-sections. Third, the background generated from the target windows, one of the dominant sources of systematic uncertainty in all previous e-p experiments, was highly suppressed in the PRad experiment.

The PRad experimental apparatus consisted of four main elements (Fig. 1). (1) A 4-cm-long windowless cryo-cooled hydrogen gas flow target with an areal density of  $2 \times 10^{18}$  atoms per  $\text{cm}^2$ , which eliminated the beam background from the target windows. (2) The high-resolution, large-acceptance hybrid electromagnetic calorimeter, HyCal<sup>20</sup>. The complete azimuthal coverage of HyCal for the forward-scattering angles enabled simultaneous detection of the pair of electrons from e-e scattering. (3) A plane made of two high-resolution X-Y gas electron multiplier (GEM) coordinate detectors located in front of HyCal. (4) A two-section vacuum chamber spanning the 5.5-m distance from the target to the detectors.

The PRad experiment was performed in Hall B at Jefferson Laboratory in May–June of 2016, using 1.1-GeV and 2.2-GeV electron beams. The standard Hall B beam line, designed for low beam currents (0.1–50 nA), was used in this experiment. The incident electrons that scattered off the target protons and the Møller electron pairs were detected in the GEM detector and HyCal. The energy and position of the detected electron(s) were measured by HyCal, and the transverse (X-Y) position was measured by the GEM detector, which was used to assign the  $Q^2$  for each detected event. The GEM detector, which has a position resolution of 72  $\mu\text{m}$ , improved the measurement accuracy of  $Q^2$  compared to detection by HyCal alone. Furthermore, the GEM detector suppressed the contamination from photons generated in the target and other beam-line materials; HyCal is equally sensitive to electrons

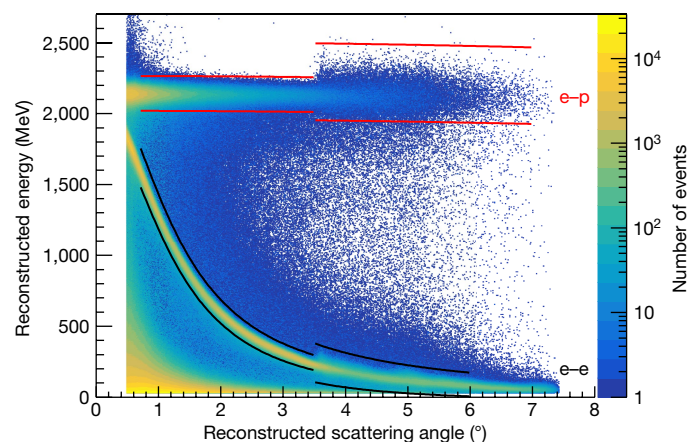


**Fig. 2 | Event reconstruction.** The reconstructed energy versus angle for e-p and e-e events for an electron beam energy of 2.2 GeV. The red and black lines indicate the event selections for e-p and e-e, respectively. The angles  $\leq 3.5^\circ$  are covered by the crystal  $\text{PbWO}_4$  modules of HyCal and the larger angles by the Pb glass modules. The colour bar shows the number of events.

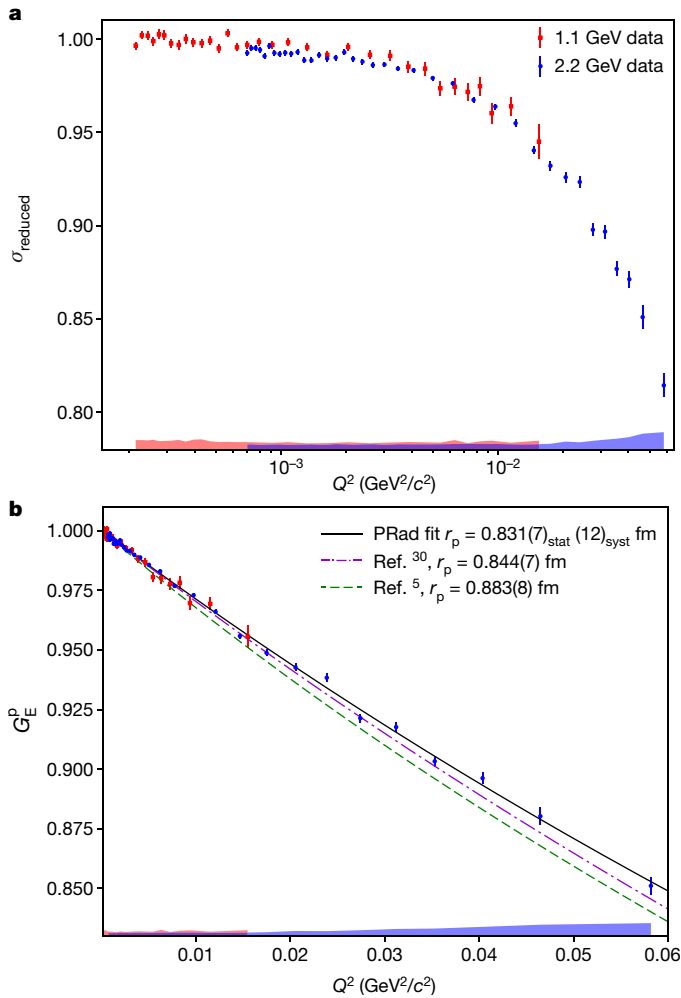


**Fig. 3 | The measured cross-section and form factor. a**, The reduced cross-section,  $\sigma_{\text{reduced}} = \left( \frac{d\sigma}{d\Omega} \right)_{e-p} / \left[ \left( \frac{d\sigma}{d\Omega} \right)_{\text{point-like}} \left( (4M_p^2 E' / E) / (4M_p^2 + Q^2) \right) \right]$ , (where  $E$  is the electron beam energy,  $E'$  is the energy of the scattered electron,  $M_p$  is the mass of the proton and  $\Omega$  is the solid angle subtended by the scattered electron detector), for the PRad e-p data. Dividing out the kinematic factor inside the square brackets,  $\sigma_{\text{reduced}}$  is a linear combination of the electromagnetic form factors squared. The bands at the bottom of the plot are the size of the systematic uncertainties, for 1.1 GeV (red) and 2.2 GeV (blue). The error bars show statistical uncertainties. **b**,  $G_E^p$  as a function of  $Q^2$ . The data points are normalized by the parameter  $n$  in equation (1) for the 1.1-GeV and 2.2-GeV data, labelled as  $n_1$  and  $n_2$ , respectively. The error bars show statistical uncertainties. The bands are the systematic uncertainties as in **a**. The solid black curve shows  $G_E^p(Q^2)$  as a fit to the function given by equation (1). Also shown is the fit from a previous e-p experiment<sup>5</sup>, giving  $r_p = 0.883(8)$  fm (green dashed line) and another previous calculation<sup>30</sup> giving  $r_p = 0.844(7)$  fm (purple dot-dashed line).

and photons, whereas the GEM detector is mostly insensitive to neutral particles. The GEM detector also helped to suppress position-dependent irregularities in the response of HyCal. A plot of the reconstructed energy versus the reconstructed angle for e-p and e-e events is shown in Fig. 2 for the 2.2-GeV beam energy.

The background was measured periodically with an empty target cell. To mimic the residual gas in the beam line,  $H_2$  gas at very low pressure was allowed in the target chamber during the empty target runs. The charge-normalized e-p and Møller scattering yields from the empty target cell were used to subtract the background contributions. The beam current was measured with the Hall B Faraday cup with an uncertainty of  $<0.1\%$ <sup>21</sup>. Further details on the background subtraction can be found in the Supplementary Information.

A comprehensive Monte Carlo simulation of the PRad setup was developed using the Geant4 toolkit<sup>22</sup>. The simulation consists of two separate event generators built for the e-p and e-e processes<sup>23,24</sup>. Inelastic e-p scattering background events were also included in the simulation using a fit<sup>25</sup> to the e-p inelastic world data. The simulation included signal digitization and photon propagation, which were critical for the precise reconstruction of the position and energy of each event in the HyCal. The details are described in the Supplementary Information.

The e-p cross-sections were obtained by comparing the simulated and measured e-p yield relative to the simulated and measured e-e yield (see Supplementary Information for details). The extracted reduced cross-section is shown in Fig. 3a. The e-p elastic cross-section is related to  $G_E^p$  and the proton magnetic form factor,  $G_M^p$ , by the Rosenbluth formula<sup>19</sup>. In the very low  $Q^2$  region covered by the PRad experiment, the cross-section is dominated by the contribution from  $G_E^p$ . Thus, the uncertainty introduced from  $G_M^p$  is negligible. In fact, when using a wide variety of parametrizations<sup>5,26-28</sup> for  $G_M^p$ , the extracted  $G_E^p$  varies by about 0.2% at  $Q^2 = 0.06$   $\text{GeV}^2/c^2$ , the largest  $Q^2$  accessed by the PRad experiment, and by  $<0.01\%$  in the  $Q^2 < 0.01$   $\text{GeV}^2/c^2$  region. The largest variation in  $r_p$  arising from the choice of  $G_M^p$  parametrization is 0.001 fm.  $G_E^p(Q^2)$  as extracted from our data is shown in Fig. 3b, using the Kelly parametrization<sup>26</sup> for  $G_M^p$ .

The slope of  $G_E^p(Q^2)$  as  $Q^2 \rightarrow 0$  is proportional to  $r_p^2$ . A common practice is to fit  $G_E^p(Q^2)$  to a functional form and to obtain  $r_p$  by extrapolating to  $Q^2 = 0$ . However, each functional form truncates the higher-order moments of  $G_E^p(Q^2)$  differently and introduces a model dependence that can bias the determination of  $r_p$ . It is critical to choose a robust functional form that is most likely to yield an unbiased estimation of  $r_p$  given the uncertainties in the data, and to test the chosen functional form over a broad range of parametrizations<sup>29</sup> of  $G_E^p(Q^2)$ . To simultaneously minimize possible bias in the determination of the radius and the total uncertainty, various functional forms were examined for their robustness in reproducing an input  $r_p$  used to generate a mock dataset with the same statistical uncertainty as the PRad data. The robustness, quantified as the root-mean square error (RMSE), is defined as  $\text{RMSE} = \sqrt{(\delta R)^2 + \sigma^2}$ , where  $\delta R$  is the bias or the difference between the input and extracted radius and  $\sigma$  is the statistical variation of the fit to the mock data<sup>29</sup>. Previous studies<sup>29</sup> show (see Supplementary Information) that consistent results with the smallest uncertainties can be achieved using a multi-parameter rational function, which we refer to as Rational(1, 1):

$$f(Q^2) = nG_E^p(Q^2) = n \frac{1 + p_1 Q^2}{1 + p_2 Q^2} \quad (1)$$

where  $n$  is the floating normalization parameter,  $p_1$  and  $p_2$  are fit parameters and the proton charge radius is given by  $r_p = \sqrt{6(p_2 - p_1)}$ . The  $G_E^p(Q^2)$ , extracted from the 1.1-GeV and 2.2-GeV data, was fitted simultaneously using the Rational(1, 1) function. Independent normalization parameters  $n_1$  and  $n_2$  were assigned for the 1.1-GeV and 2.2-GeV data, respectively, to allow for differences in normalization uncertainties, but the  $Q^2$  dependence was identical. The parameters obtained from fits to the Rational(1, 1) function are  $n_1 = 1.0002 \pm 0.0002_{\text{stat}} \pm 0.0020_{\text{syst}}$ ;  $n_2 = 0.9983 \pm 0.0002_{\text{stat}} \pm 0.0013_{\text{syst}}$ ; and  $r_p = 0.831 \pm 0.007_{\text{stat}} \pm 0.012_{\text{syst}}$  fm. The Rational(1, 1) function describes the data very well, with a reduced  $\chi^2$  of 1.3 when considering only the statistical uncertainty. The values of  $r_p$  for a variety of functional forms fitted to the PRad data are shown in Supplementary Fig. 15.

To determine the systematic uncertainty in  $r_p$ , a Monte Carlo technique was used to randomly smear the cross-section and  $G_E^p(Q^2)$  data points for each known source of systematic uncertainty. The value of  $r_p$  was extracted from the smeared data and the process was repeated 100,000 times. The root-mean square of the resulting distribution of  $r_p$  is recorded as the systematic uncertainty. The dominant systematic uncertainties of  $r_p$  are those that are  $Q^2$ -dependent, which primarily affect the lowest  $Q^2$  data: the Møller radiative corrections, the background subtraction for the

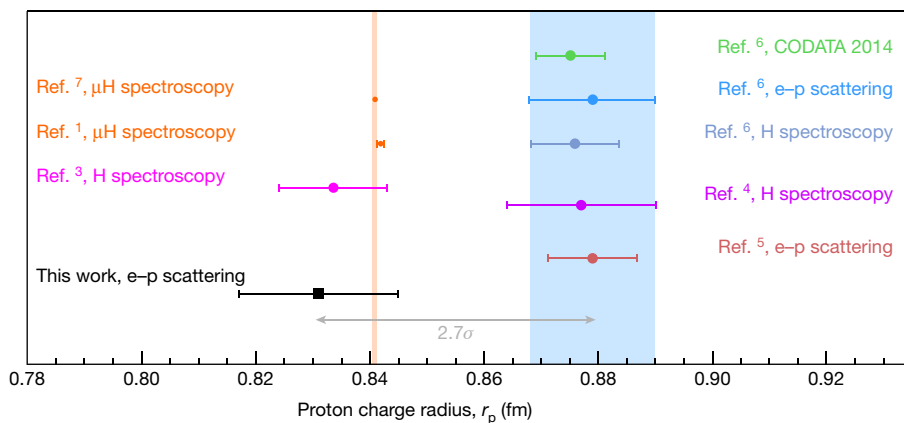


**Fig. 4 | The proton charge radius,  $r_p$ , as extracted from the PRad data in this work, shown alongside other measurements of  $r_p$  since 2010 and previous CODATA recommended values. Our result is 2.7 $\sigma$  smaller than the CODATA recommended value for e-p experiments<sup>6</sup>. The orange and blue vertical bands show the uncertainty bounds of the  $\mu$ H and CODATA values for e-p scattering, respectively.**

1.1-GeV data and event selection. The uncertainty in  $r_p$  arising from the finite  $Q^2$  range and the extrapolation to  $Q^2 = 0$  was investigated by varying the  $Q^2$  range of the mock dataset as part of the robustness study of the Rational(1, 1) function<sup>29</sup>. This uncertainty was found to be much smaller than the relative statistical uncertainty, 0.8%. The total systematic relative uncertainty on  $r_p$  was found to be 1.4%, and is detailed in Supplementary Table 1 and described in the Supplementary Information.

The value of  $r_p$  obtained using the Rational(1, 1) function is shown in Fig. 4, with statistical and systematic uncertainties summed in quadrature. Our result, obtained from  $Q^2$  down to an unprecedented  $2.1 \times 10^{-4} \text{ GeV}^2/c^2$ , is about three standard deviations smaller than the previous high-precision electron scattering measurement<sup>5</sup>, which was limited to higher  $Q^2$  ( $>0.004 \text{ GeV}^2/c^2$ ). However, our result is consistent with the  $\mu$ H Lamb-shift measurements<sup>1,7</sup>, and also with the recent 2S-4P transition-frequency measurement using ordinary H atoms<sup>3</sup>. Given that the lowest  $Q^2$  reached in the PRad experiment is an order of magnitude lower than in previous e-p experiments, and owing to the careful control of systematic effects, our result indicates that the proton radius is smaller than its previously accepted value from e-p measurements. Our result does not support any fundamental difference between e-p and  $\mu$ -p interactions and is consistent with the updated value announced for the Rydberg constant by CODATA<sup>8</sup>.

The PRad e-p experiment covers  $Q^2$  over two orders of magnitude in one setting. The experiment also exploited the simultaneous detection of e-p and e-e scattering to achieve good control of systematic uncertainties, which were, by design, different from previous e-p experiments. The extraction of  $r_p$  using functional forms with validated robustness is another strength of this result. Our result demonstrates a large discrepancy with contemporary, high-precision e-p experiments. The result also implies that there is consistency between proton charge radii as obtained from e-p scattering measurements on ordinary hydrogen and spectroscopy of muonic hydrogen<sup>1,7</sup>. The PRad experiment demonstrates the clear advantages of the calorimeter-based method for determining  $r_p$  from e-p experiments and points to further possible improvements in the accuracy of this method. It is also consistent with the recently announced shift in the Rydberg constant<sup>8</sup>, which has profound consequences, given that the Rydberg constant is one of the most precisely known constants of physics.

**Online content**

Any methods, additional references, Nature Research reporting summaries, source data, extended data, supplementary information, acknowledgements, peer review information; details of author contributions and competing interests; and statements of data and code availability are available at <https://doi.org/10.1038/s41586-019-1721-2>.

3. Beyer, A. et al. The Rydberg constant and proton size from atomic hydrogen. *Science* **358**, 79–85 (2017).
4. Fleurbaey, H. New measurement of the 1S–3S transition frequency of hydrogen: contribution to the proton charge radius puzzle. *Phys. Rev. Lett.* **120**, 183001 (2018).
5. Bernauer, J. C. et al. High-precision determination of the electric and magnetic form factors of the proton. *Phys. Rev. Lett.* **105**, 242001 (2010).
6. Mohr, P. J., Newell, D. B. & Taylor, B. N. CODATA recommended values of the fundamental physical constants: 2014. *J. Phys. Chem. Ref. Data* **45**, 043102 (2016).
7. Antognini, A. et al. Proton structure from the measurement of 2S–2P transition frequencies of muonic hydrogen. *Science* **339**, 417–420 (2013).
8. Mohr, P. J., Newell, D. B. & Taylor, B. N. CODATA recommended values of the fundamental physical constants: 2018. <http://physics.nist.gov/constants> (2019).
9. Hasan, N. et al. Computing the nucleon charge and axial radii directly at  $Q^2 = 0$  in lattice QCD. *Phys. Rev. D* **97**, 034504 (2018).
10. Mohr, P. J., Taylor, B. N. & Newell, D. B. CODATA recommended values of the fundamental physical constants: 2010. *Rev. Mod. Phys.* **84**, 1527–1605 (2012).
11. Carlson, C. E. The proton radius puzzle. *Prog. Part. Nucl. Phys.* **82**, 59–77 (2015).
12. Liu, Y. S. & Miller, G. A. Validity of the Weizsäcker–Williams approximation and the analysis of beam dump experiments: production of an axion, a dark photon, or a new axial-vector boson. *Phys. Rev. D* **96**, 016004 (2017).
13. Miller, G. A. Defining the proton radius: a unified treatment. *Phys. Rev. C* **99**, 035202 (2019).
14. Miller, G. A. Proton polarizability contribution: muonic hydrogen Lamb shift and elastic scattering. *Phys. Lett. B* **718**, 1078–1082 (2013).
15. Antognini, A. et al. Theory of the 2S–2P Lamb shift and 2S hyperfine splitting in muonic hydrogen. *Ann. Phys.* **331**, 127–145 (2013).
16. Lee, G., Arrington, J. R. & Hill, R. J. Extraction of the proton radius from electron–proton scattering data. *Phys. Rev. D* **92**, 013013 (2015).
17. Higinbotham, D. W. et al. Proton radius from electron scattering data. *Phys. Rev. C* **93**, 055207 (2016).
18. Griffioen, K., Carlson, C. & Maddox, S. Consistency of electron scattering data with a small proton radius. *Phys. Rev. C* **93**, 065207 (2016).
19. Gasparian, A. et al. *High Precision Measurement of the Proton Charge Radius*. Proposal to Jefferson Lab, PAC-38 C12-11-106 [https://www.jlab.org/exp\\_prog/proposals/11/PR12-11-106.pdf](https://www.jlab.org/exp_prog/proposals/11/PR12-11-106.pdf) (2011).
20. Gasparian, A. A high performance hybrid electromagnetic calorimeter at Jefferson Lab. In *Proc. 11th Int. Conf. on Calorimetry in Particle Physics* (eds Cecchi, C. et al.) 109–115 (World Scientific, 2005).
21. Mecking, B. et al. The CEBAF large acceptance spectrometer (CLAS). *Nucl. Instrum. Meth. A* **503**, 513–553 (2003).
22. Agostinelli, S. et al. GEANT4: a simulation toolkit. *Nucl. Instrum. Meth. A* **506**, 250–303 (2003).
23. Akushevich, I., Gao, H., Ilyichev, A. & Meziane, M. Radiative corrections beyond the ultra relativistic limit in unpolarized ep elastic and Møller scatterings for the PRad experiment at Jefferson Laboratory. *Eur. Phys. J. A* **51**, 1 (2015).
24. Gramolin, A. V. et al. A new event generator for the elastic scattering of charged leptons on protons. *J. Phys. G Nucl. Phys.* **41**, 115001 (2014).
25. Christy, M. E. & Bosted, P. E. Empirical fit to precision inclusive electron–proton cross-sections in the resonance region. *Phys. Rev. C* **81**, 055213 (2010).
26. Kelly, J. J. Simple parametrization of nucleon form factors. *Phys. Rev. C* **70**, 068202 (2004).
27. Venkat, S., Arrington, J., Miller, G. A. & Zhan, X. Realistic transverse images of the proton charge and magnetic densities. *Phys. Rev. C* **83**, 015203 (2011).
28. Higinbotham, D. W. & McClellan, R. E. How analytic choices can affect the extraction of electromagnetic form factors from elastic electron scattering cross section data. Preprint at <https://arxiv.org/abs/1902.08185> (2018).
29. Yan, X. et al. Robust extraction of the proton charge radius from electron–proton scattering data. *Phys. Rev. C* **98**, 025204 (2018).
30. Alarcón, J. M., Higinbotham, D. W., Weiss, C. & Ye, Z. Proton charge radius from electron scattering data using dispersively improved chiral effective field theory. *Phys. Rev. C* **99**, 044303 (2019).

**Publisher’s note** Springer Nature remains neutral with regard to jurisdictional claims in published maps and institutional affiliations.

© This is a U.S. government work and not under copyright protection in the U.S.; foreign copyright protection may apply 2019

## Methods

The PRad experiment was conducted with 1.1-GeV and 2.2-GeV electron beams from the Continuous Electron Beam Accelerator Facility (CEBAF) accelerator incident on cold hydrogen atoms flowing through a windowless target cell. The scattered electrons, after traversing the vacuum chamber, were detected in the GEM detector and HyCal. They included electrons from elastic e–p scattering and e–e Møller scattering processes. The transverse ( $X$ – $Y$ ) positions measured by the GEM detector were used to calculate the  $Q^2$  value for each event. The e–p and e–e yields were obtained using appropriate cuts on the energy deposited in HyCal and the reconstructed angle. The e–p and e–e yields were binned as a function of  $Q^2$ . A comprehensive Monte Carlo simulation of the PRad experiment was used to extract the next-to-leading order e–p cross-section from the experimental yields. The e–p cross-sections were obtained by comparing the simulated and measured e–p yield relative to the simulated and measured Møller scattering yield. The value of  $G_E^p$  was extracted from the e–p cross-section using the Rosenbluth formula, and using a parametrization of  $G_M^p$ . The proton charge radius,  $r_p$ , was obtained from the extracted  $G_E^p(Q^2)$  by fitting to the Rational(1, 1) functional form and extrapolating to  $Q^2 = 0$ . The Rational(1, 1) functional form was shown to be the most robust function for radius extraction from the PRad data, giving consistent results with the smallest uncertainties. See Supplementary Information for further details.

## Data availability

The raw data from this experiment are archived in Jefferson Laboratory's mass storage silo.

## Code availability

All computer codes used for data analysis and simulation are archived in Jefferson Laboratory's mass storage silo.

**Acknowledgements** This work was funded in part by the US National Science Foundation (NSF MRI PHY-1229153) and by the US Department of Energy (contract number DE-FG02-03ER41231), including contract number DE-AC05-06OR23177, under which Jefferson Science Associates, LLC operates the Thomas Jefferson National Accelerator Facility. We thank the staff of Jefferson Laboratory for their support throughout the experiment. We are also grateful to all grant agencies for providing funding support to the authors throughout this project. We acknowledge discussions about radiative corrections with A. Afanasev, I. Akushevich, A. V. Gramolin and O. Tomalak. We thank S. Danagoulian for helping to restore the light monitoring system of HyCal. We also thank S. Javalkar for help with a beam halo study.

**Author contributions** A.G. is the spokesperson of the experiment. H.G., D. Dutta and M.K. are co-spokespersons of the experiment. A.G. developed the initial concepts of the experiment. A.G., H.G., D. Dutta and M.K. designed and proposed the experiment. The entire PRad collaboration constructed the experiment and worked on the data collection. The COMSOL simulation of the target was built by Y.Z. The Monte Carlo simulation was built and validated by C. Peng, C.G., W.X. and X.B. with input from numerous other members of the collaboration. Calibrations were carried out by W.X., M.L., X.B., C. Peng, L.Y. and X.Y., with input from I.L. Analysis software tools were developed by C. Peng, with input from X.B., M.L., I.L., L.Y., W.X. and X.Y. The data analysis was carried out by W.X., C. Peng, X.B., M.L. and C.G., with input from A.G., H.G., D. Dutta, M.K., N.L., E.P., X.Y., D.W.H., L.Y. and M.L.K. All authors reviewed the manuscript.

**Competing interests** The authors declare no competing interests.

## Additional information

**Supplementary information** is available for this paper at <https://doi.org/10.1038/s41586-019-1721-2>.

**Correspondence and requests for materials** should be addressed to A.G. or D.D.

**Peer review information** *Nature* thanks Krzysztof Pachucki and the other, anonymous, reviewer(s) for their contribution to the peer review of this work.

**Reprints and permissions information** is available at <http://www.nature.com/reprints>.